Water permeation and wavelike density distributions inside narrow nanochannels

Hangjun Lu,[1,2,3] Jingyuan Li,[4] Xiaojing Gong,[1] Rongzheng Wan,[1] Li Zeng,[1] and Haiping Fang[1,5,*]
[1]*Shanghai Institute of Applied Physics, Chinese Academy of Sciences, Shanghai 201800, People's Republic of China*
[2]*Graduate School of the Chinese Academy of Sciences, Beijing 100080, People's Republic of China*
[3]*Department of Physics, Zhejiang Normal University, Jinhua 321004, People's Republic of China*
[4]*Department of Physics, Zhejiang University, Hangzhou 310027, People's Republic of China*
[5]*Theoretical Physics Center for Science Facilities (TPCSF), CAS, 19(B) Yuquan Road, Beijing 100049, People's Republic of China*
(Received 23 August 2007; revised manuscript received 30 April 2008; published 23 May 2008)

When water is confined in narrow nanochannels with appropriate radii, the water molecules form single files. Here, the gating of water permeation across such nanochannels under continuous deformations and the pattern of the density distribution of water inside are studied by molecular dynamics simulations. When the number of water molecules inside the channel is close to an integer and half, although there is no clearly wavelike pattern for the water density distribution near the center of the channel, we find that the water density distribution, from the data collected with a fixed number of water molecules inside the nanochannel, still shows a clear wavelike pattern. The behavior for the changes in those wavelike water density distributions is found to be consistent with the gating of the water permeation with respect to the channel deformation. A simple theoretical model is proposed to exploit the physical origin of the wavelike patterns. We find that the potential barriers at both ends together with the tight hydrogen-bonding network are the main responsibility. These findings indicate that both the gating and wavelike pattern are independent of the length of the nanochannels and are helpful to understand similar phenomena in biological channels and other nanoscale pores.

DOI: 10.1103/PhysRevB.77.174115 PACS number(s): 81.07.De, 66.10.C−, 66.20.−d, 66.25.+g

I. INTRODUCTION

Since the synthesis of carbon nanotubes (CNTs) in 1991,[1] it has been recognized by both computer simulations and experiments that CNTs have a wide range of potential applications, such as molecular sieves,[2,3] nanotube membranes,[4] sensors,[5] minute chemical reactors,[6] and nanofluidic devices for the precise delivery of gases, liquids, medicine, and biological molecules.[7–13] Recently, it has been found that water confined in nanotubes usually exhibits dynamics different from bulk water.[14–17] Carbon nanotubes have also been used as model systems to exploit some of the primary behaviors of the complex biological water channels.[18–21] It has been found that the single-file arrangement, wavelike density distribution, and wet-dry transitions due to confinement are shared by CNTs with appropriate radii and the biological channels.[22–28]

It is well known that the density distribution is a constant along a macroscopic channel with a uniform radius if there is no pressure difference between the ends of the channel. However, wavelike patterns of the water density distributions have been found in a carbon nanotube with 8.1 Å in diameter and 13.4 Å in length, where the water molecules inside the channel form single-file structure.[29] The average number of water molecules inside the nanotube is very close to an integer of 5. Further, the gating of the water permeation across this carbon nanotube was found to be related to the wavelike pattern of water density distribution.[20] However, the physical origin of the wavelike pattern and its response to the deformation of the carbon nanotube are still unclear. Moreover, it is found that if the length of the carbon nanotube is a little larger, say, 14.6 Å, the wavelike pattern of water density distribution near the center of this channel becomes much weaker (see Fig. 2). This raises more interests on the origin of the wavelike pattern of water density distribution inside the channel, how the water density distribution changes with respect to the length of the channel, and whether the gating still exists for longer CNTs.

In this work, we present an approach toward those questions. Water transportation through a CNT with 14.6 Å in length under continuous deformations is studied with molecular dynamics simulations. In this system, the excellent on-off gating of the water permeation can be still observed. We find that the water density distribution still shows a clear wavelike pattern if we only collect the data from simulations with a fixed number of water molecules inside the nanochannel. The excellent on-off gating of the water permeation is correlated with the behavior for the changes in those wavelike water density distributions. We also present a theoretical model to describe the water density distributions and its change with respect to the deformation of the channel. We find that the wavelike patterns of the water density distributions mainly result from the potential barriers at both ends of the nanochannel together with the tight hydrogen-bonding network inside the tube, which fixes the distance between the two neighboring water molecules inside the channel approximately.

This paper is organized as follows. The simulation model and parameters are introduced in Sec. II. Section III devotes to the simulation results and discussion. In Sec. IV, a simple theoretical model is introduced to elucidate the physical origin of the wavelike patterns of the water density distributions. Finally, conclusions are presented in Sec. V.

II. METHODOLOGY

The simulation framework is shown in Fig. 1. A single graphite sheet divides the full space into two parts. An un-

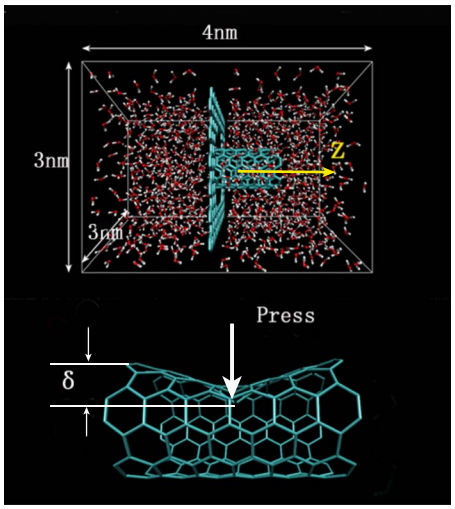

FIG. 1. (Color online) Snapshot of the simulation system. The CNT and the graphite sheet are solvated in a box ($3\times3\times4$ nm^3) with 1036 water molecules. The nanotube of the simulation setup is amplified. An external force, marked by press, acts on an atom of the carbon nanotube and a deformation can be clearly seen. δ is the displacement of the forced atom from its initial equilibrium position.

capped, single-walled carbon nanotube,[30] 14.6 Å in length and 8.1 Å in diameter, along the z direction is embedded in the center of a graphite sheet. The distance between the left end of the CNT and the graphite sheet is 2 Å. The 156-carbon (6, 6) nanotube is formed by folding a graphite sheet of 5.5×12 carbon rings to a cylinder. Correspondingly, the number of carbon rings along the nanotube is 5.5, which is 0.5 ring longer than the CNT used in our previous paper.[20] The CNT is relaxed with the interaction between carbon atoms, which is described with the parametrized potential by Brenner[31] according to the Tersoff formulism.[32] Periodic boundary conditions are applied in all directions. A force is applied to one carbon atom (the forced atom) in the top side of the carbon nanotube. The carbon atoms in the bottom half of the carbon nanotube are fixed. Consequently, this atom, together with some of its neighboring carbon atoms, is pushed away from their initial positions. For each external force, an equilibrium state $\mathfrak{R}$ of a CNT can be obtained by relaxation and corresponds to a displacement of the forced atom denoted by δ.

When two sides of a membrane have the same hydrostatic pressure but different concentrations of an impermeable solute, an osmotic pressure difference is established and water flows from the side with lower solute concentration to the other side. Following the method proposed by Zhu *et al.*[33] and our previous paper,[20,21] an external force is applied to each water molecule along the $+z$ direction to obtain a pressure difference between the two ends of the CNT. Similar method was used by Joseph and Aluru.[34] This pressure difference is something like the osmotic pressure difference[23,33] and is 133 MPa between the two ends of the CNT for an additional acceleration of 0.1 nm ps^{-2} at each atom. In order to prevent the CNT from being swept away, the carbon atoms at the inlet and outlet are fixed up in the simulations by position restraint with spring constant of 300 000 kJ mol^{-1} nm^{-2}.

The molecular dynamics simulations were carried out at a constant pressure (1 bar with initial box sizes of L_x=3.0 nm, L_y=3.0 nm, and L_z=4.0 nm) and temperature (300 K) with GROMACS3.2.1.[35] Barostat and thermostat of Berendsen *et al.*[36] with a time constant of 0.5 ps were used. Electrostatic and Lennard-Jones interactions were computed by using cutoff with the cutoff radii of 1.0 nm. Here, the TIP3P water model[37] was applied. A time step of 2 fs was used and data were collected every 0.5 ps. In the simulations, the carbon atoms are modeled as uncharged Lennard-Jones particles with cross sections of σ_{CC}=0.34 nm and σ_{CO} =0.3275 nm and depths of the potential well of ε_{CC} =0.3612 kJ mol^{-1} and ε_{CO}=0.4802 kJ mol^{-1}. Carbon-carbon bond lengths of 0.14 nm and bond angles of 120° are maintained by harmonic potentials with spring constants of 393 960 kJ mol^{-1} nm^{-2} and 527 kJ mol^{-1} rad^{-2} before relaxation. In addition, a weak dihedral angle potential is applied to the bonded carbon atoms.

In the computation of $\rho(z)$, we extended the CNT from each end to bulk by 11.3 Å to construct a virtual cylinder of 36 Å in length and 8.1 Å in diameter. The cylinder was divided into 1000 bins. The water density can be calculated by $\rho(z)=\frac{N(z)}{N}\frac{1}{\Delta L}$, where ΔL is the bin length and $N(z)$ is the number of water molecules appearing at the bin at z for the total of N snapshots from simulation.

III. RESULTS AND DISCUSSION

For each state $\mathfrak{R}$, corresponding to a displacement δ, the time for the numerical simulation is 122 ns. The last 120 ns of the simulation were collected for analysis. Initially, water molecules were filled in the other space of the system except for the channel of the CNT. For each simulation, the nanotube is rapidly filled by water from the surrounding reservoir.

The water density distributions along the z direction under different values of δ are shown in Fig. 2. The red and black filled circles denote the locations of the carbon atoms. Different from our previous results in Ref. 20 with a shorter CNT, the wavelike pattern is quite flat near the center of the channel for the unperturbed nanotube. Even near the openings, the wavelike patterns are less obvious than those in Ref. 20. The peak-peak value is only 0.05 Å^{-1} computed from the first peak and dip from the left end, which is much smaller than the average peak-peak value of 0.12 Å^{-1} in Ref. 20.

The structure of wavelike pattern is not only sensitive to the length of the CNT but also to the shape of the CNT. It is remarkable to find that the wavelike pattern of water density distribution becomes obvious and shifts slightly when the CNT is under continuous deformations. From δ=0 to 1.5 Å, the amplitude of the wave pattern shows a clear increase, but the distances between crests and troughs (wavelength) keep almost fixed. For 1.5 Å, $<\delta\leq\delta_c\approx2.0$ Å, the amplitude of the wave pattern increases sharply, but the wave pattern still keeps well. From $\delta\approx2.1$ Å and up, the water density distribution at P is smaller than those of the other dips. For $\delta\geq2.5$ Å, the distribution at P is very close to zero.

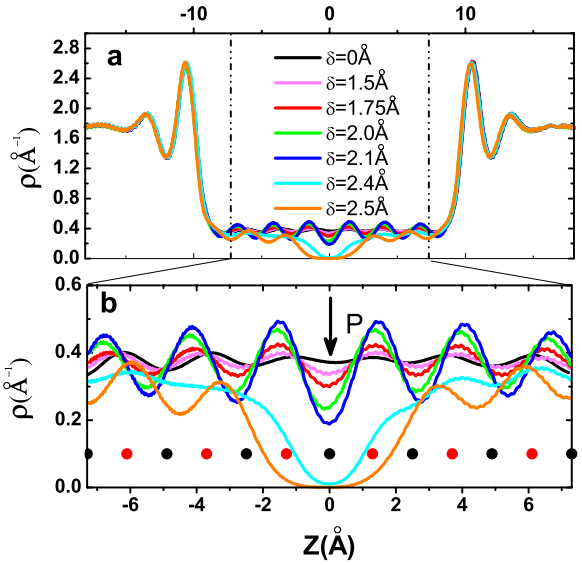

FIG. 2. (Color online) (a) Water density distributions along the nanotube axis for δ=0, 1.5, 1.75, 2.0, 2.1, 2.4, 2.5 Å. (b) Water density distribution inside the nanotube together with the positions of carbon atoms. The red and black filled circles denote the locations of the carbon atoms. The arrow, marked by P, is the position of the atom affected by an external force.

The flux and the average number of water molecules inside the tube $\langle N\rangle$ under different values of δ are shown in Fig. 3. In this paper, the flux is defined by the difference of the numbers of water molecules entered the CNT from left and right ends, left on the other sides, per nanosecond.[20,21] For the unperturbed CNT, the average number of water molecules $\langle N\rangle$ is about 5.5. The flux, correspondingly, is about 5.4 water molecules/ns from the left to the right through the CNT, which is very close to 5.7 ns^{-1} for the CNT with five rings[20] and comparable to the measured 3.9 ± 0.6 ns^{-1} for aquaporin-1.[38] Similar to the case for the CNT with five rings,[20] excellent on-off gating behavior is also observed. The flux and $\langle N\rangle$ are almost unchanged when δ is less than 2.0 Å. However, they decrease dramatically as δ is above the critical value, $\delta_c \approx 2.0$ Å (see Fig. 3). For δ=2.5 Å, the water flux is close to zero and $\langle N\rangle$ decreases to about 3. The

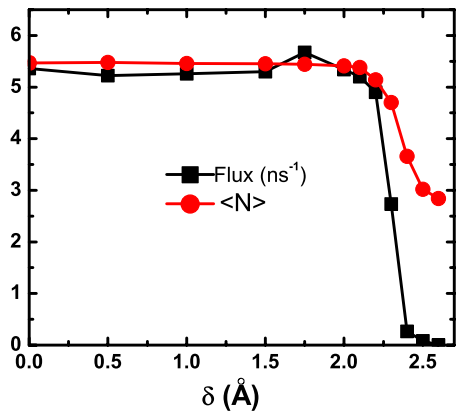

FIG. 3. (Color online) Average value of number N of the water molecules inside the tube and the water flux for different δ.

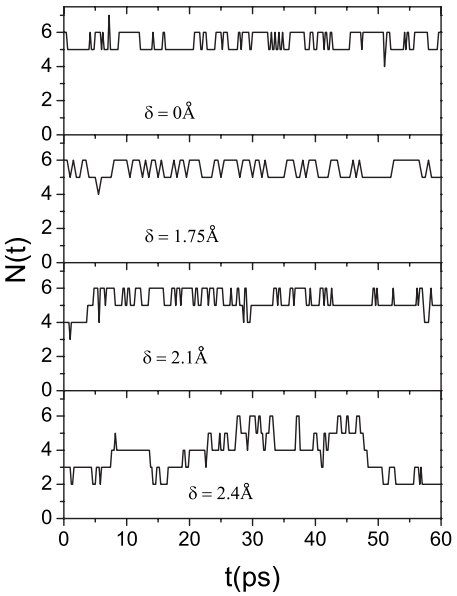

FIG. 4. Number of water molecules N inside the nanotube as a function of time in several representative systems with δ=0, 1.75, 2.1, and 2.4 Å.

channel switches from an open state to a closed state. The value of δ_c is consistent with our previous paper[20] and not affected by the length of the CNT.

Figure 4 shows the number N of water molecules inside the CNT as a function of time for different δ. The channel predominantly contains either 5 or 6 water molecules for $\delta \leq \delta_c$, i.e., there are two stable states with N=5 and N=6. The system switches mainly between the two states. For the unperturbed CNT, we find that the average durations for the states with N=5 and N=6 are 0.96 and 0.90 ps, respectively, showing similar probabilities for those two states.

In Fig. 5, we show the free energy of occupancy fluctuations $G(N)$, $G(N)=-k_BT \ln p(N)$, where $p(N)$ is the probability of finding exactly N water molecules inside the nanotube, k_B the is Boltzmann constant, and T is the temperature. Different from the observation in our previous paper[20] and work of Hummer *et al.*,[29] the free energy of N=6 for the unperturbed CNT is nearly equal to the free energy of N=5 for $\delta \leq \delta_c$, which is consistent with the above observation that the average durations for the states with N=5 and N=6 are

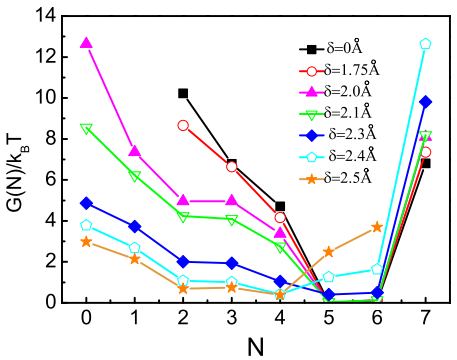

FIG. 5. (Color online) Free energy of occupancy fluctuation, $G(N)$, for δ=0, 1.75, 2.0, 2.1, 2.3, 2.4, and 2.5 Å.

very close. The rapid transitions between the two states in the water permeation across the channel are quite similar to that observed in the KcsA ion channel.[39] As δ further increases, say, δ=2.4 Å, the behavior becomes quite different. In most of the time, the number of water molecules is neither 5 nor 6.

From above results, we can see that the behavior of the excellent gating of water permeation across the CNT with 5.5 rings is almost the same as that of the CNT with five rings. Similar to the previous observation, there is the same critical value of the deformation parameter $\delta_c \approx 2.0$ Å, at which the net flux begins to show quick decrease and the water density distribution becomes deformed from a wavelike pattern. However, the behavior of water density distribution inside the CNT is quite different. Now, we show that why the water density distribution is so flat for the unperturbed nanochannel and the wavelike pattern becomes obvious as δ increases.

From simulation results, we find that N fluctuates between 1 and 7. The probability of N=7 is always less than 0.1% in our simulations. Thus, we only calculated the water density distributions alone the z axis for $1 \leq N \leq 6$.

When δ=0 Å, the total probability for $N>6$ and for $N \leq 4$ is only about 0.3%. The probabilities of N=5,6 are about 52% and 48%, both close to 50%. From our simulation results, we can see that the water density distributions of N=5 and N=6 show obvious wavelike pattern, as shown in Fig. 6. The average amplitude (value of peak to peak) is about 0.32 Å^{-1}, which is larger than the value of 0.12 Å^{-1} in the CNT with a shorten length.[20] For both states of N=5 and N=6, the distances between troughs and crests of the waves (wavelength) are about 2.6 Å, showing the hydrogen bonds are strong enough to keep an almost constant distance between the neighboring water molecules. The phase difference between the two waves of N=6 and N=5 is found to be about $\frac{1}{2}$ period. Thus, the total water density distribution becomes flat from the superposition of those two cases, especially in the middle region.

When the CNT is deformed by the external force exerted on the forced atom, the distribution patterns change correspondingly. In the case of δ=1.75 Å, the probabilities of N=4,5,6 are about 0.6%, 48%, and 51%, respectively, and the probabilities of N of other values are negligibly small. As shown in Fig. 6, the wavelike pattern of N=6 is almost the same as that for δ=0, while the amplitude of N=5 becomes smaller. Thus, the total water density distribution shows a wavelike pattern.

In the case of δ=2.1 Å, the probabilities of N=4,5,6 are about 2%, 51%, and 46%, respectively. The probabilities of all the other values of N are less than 1%, which is still very small. The profile of water density distribution of N=6 is only slightly modified, so the tops of the curve become sharp (see Fig. 6). However, the water density distribution of N=5 becomes flat. The total water density distribution still has a wavelike pattern, but the value at z=0 is considerably small due to the clear reduced value at z=0 for the density distribution of N=5. For δ=2.4 Å, there are clear valleys in the region of -2 Å$<z<2$ Å for all the cases of N, resulting in a big valley in the total water density distribution.

We note that the water density distribution $\rho(z)$ is related to the potential of mean forces (PMFs) by

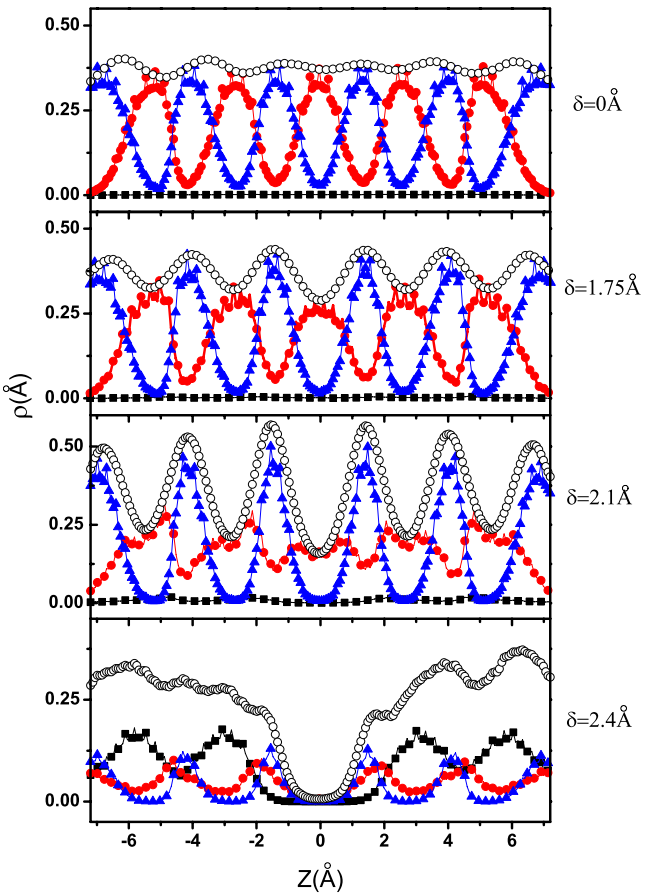

FIG. 6. (Color online) Water density distributions along the nanotube axis for N=4 (black filled squares), N=5 (red filled circles), N=6 (blue filled triangles), and the total water density distribution (open circles). The probabilities of $N<4$ and $N>6$ are negligible.

$G(z)=-k_BT \ln[\rho(z)/\rho_0]$, where ρ_0 is bulk water density.[40] PMF is often used to characterize the behavior of water molecules inside the channel. Figure 7 displays the PMF curves of water molecules along the axis of the nanotube. It is clear that any change in the water density distribution corresponds to a change in the PMF. Thus, the above discussions can also be easily explained as the behavior of the water permeation

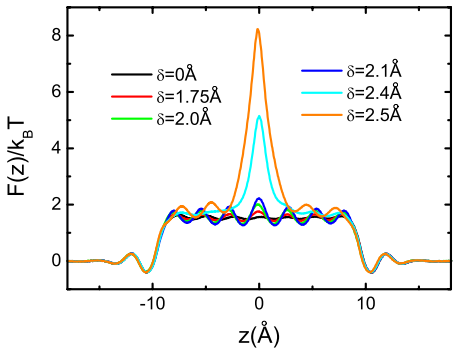

FIG. 7. (Color online) Potential of mean force $G(z)$ profiles for water along the axis of the nanotube for δ=0, 1.75, 2.0, 2.1, 2.4, and 2.5 Å.

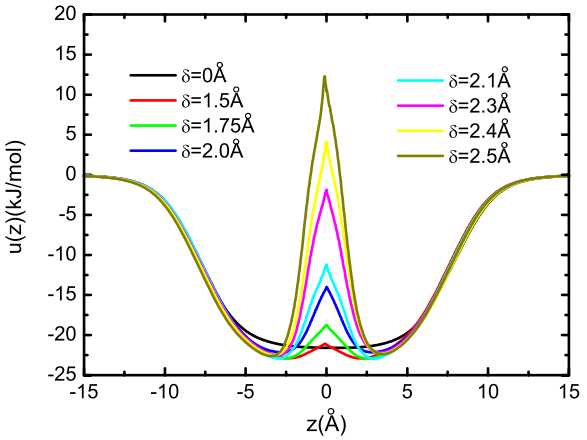

FIG. 8. (Color online) Interaction energies $u(z)$ of a water molecule at z with the carbon nanotube for different δ. The inset shows a water molecule locating at the center of the cross section at z of the carbon nanotube.

across the channel with respect to the potential. When $\delta > \delta_c$, a clear potential barrier forms around $z=0$ and the barrier increases sharply as δ increases, resulting in a rapid decrease in the net flux.

The decreasing of the water density and increasing of the PMF at $z=0$ can be understood further from the interaction energies of the water molecules with the channel. Water-CNT interaction, $u(z)$, is calculated by $u(z)=4\varepsilon_{\mathrm{CO}}\Sigma_{i=1}^{156}[(\frac{\sigma_{\mathrm{CO}}}{r_i})^{12}-(\frac{\sigma_{\mathrm{CO}}}{r_i})^{6}]$, where r_i is the distance between the water molecule and the ith carbon atom. In the calculation, we assume that the water molecule at z locates at the center of the cross section of the nanotube. The results are shown in Fig. 8. It is clear that the behavior of the potential at $z=0$ with respect to the deformation parameter δ is quite similar to that of the PMF. $u(z)$ near $z=0$ increase slowly for $\delta \leq \delta_c$ and quickly for $\delta > \delta_c$. Here, the sharp peaks result from that the external force is exerted on only one carbon atom of the CNT so that the center of the CNT at the forced atom has a sharp displacement along the direction of the external force. In the numerical simulation, water can stay near this point so that the peaks of PMF profiles are much less sharp.

Water molecules confined in the nanotube form a zigzag single-file chain (shown in Fig. 9, top panel). The distance between the two water molecules nearest neighboring the forced atom, usually one left to the forced atom and the other right to the forced atom, increases as the deformation parameter δ increases. We have computed the average distance between them, d_{WW}, and the average distance along the z direction, z_{WW}, for different δ, which are shown in Fig. 9 (bottom). When $\delta=0$, there is nothing special about d_{WW}—the distances between any two neighboring water molecules inside the channel share the same values, so does the z_{WW}. Both d_{WW} and z_{WW} increase slowly for $\delta \leq \delta_c$ and quickly for $\delta > \delta_c$, as that of the potential $u(z)$ at $z=0$. We note that when z_{WW} is larger enough, the hydrogen bond formed between the two water molecules nearest neighboring the forced atom is broken, which makes it very difficult for a water molecules passing the position facing the forced

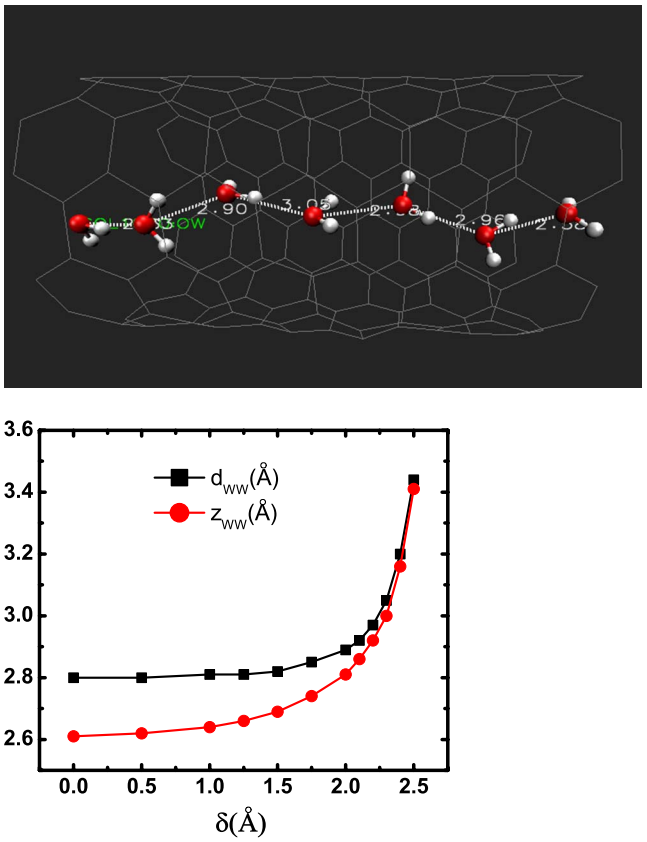

FIG. 9. (Color online) (Top) water molecules confined in the nanotube form a zigzag single-file chain. (Bottom) distance between the two water molecules near the forced atom d_{WW} and its z-projection Z_{WW} for different δ.

atom. Consequently, the flux decreases sharply as $\delta > \delta_c$. It is clear that the larger the value of z_{WW}, the smaller the water density and the larger the PMF near $z=0$.

The microscopic mechanism of excellent on-off gating with deformation signals can also be understood roughly from the evaluation below. In our simulation system, the van der Waals radius of carbon atom is 1.7 Å. The nanotube diameter at the deformation is roughly $d=d_0-2\sigma_{\mathrm{CC}}-\delta=4.7-\delta$ Å, where $d_0=8.1$ Å is the initial diameter of the CNT. Considering that when the deformation is about 2.5 Å, the channel is closed. At 2.5 Å, the width in the channel becomes $4.7-2.5=2.2$ Å, which is much smaller than the diameter of a water molecule (~2.8 Å). In the work of Beckstein *et al.*,[25] they studied that the decrease in hydrophobic pore radius induces switching from an open to a closed state. In our paper, only one carbon atom of the channel is pressed, the displacements of the other channel carbon atoms are smaller or negligible. Consequently, the critical value of the minimal width in the channel (the distance from the forced atom to the carbon atom at the corresponding position in the other half of the channel) is smaller than the critical pore radius in the work of Beckstein *et al.*[25]

In our simulations, the same external force was applied on all water molecules to study the permeation of water through the CNT. Similar method has been used in a recent paper by Joseph and Aluru.[34] To evaluate the difference between equi-

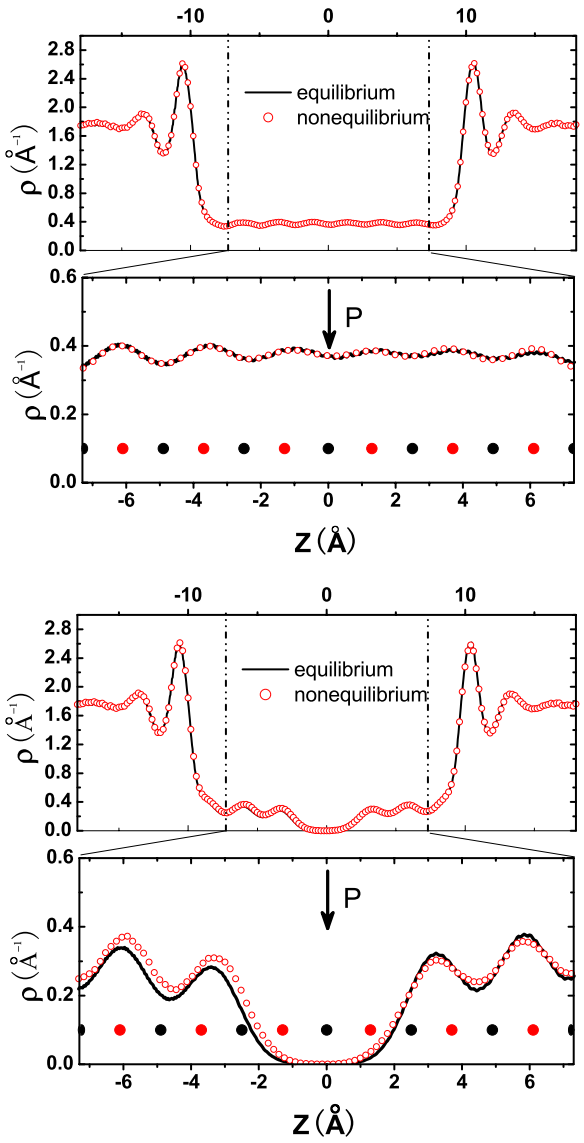

FIG. 10. (Color online) Water density distributions along the nanotube axis with or without the external artificial osmotic pressure for δ=0 Å and δ=2.5 Å. The red and black filled circles denote the locations of the carbon atoms. The arrow, marked by P, is the position of the atom affected by an external force.

librium (without artificial osmotic pressure) and nonequilibrium (with artificial osmotic pressure), we also simulated two typical system for δ=0 and δ=2.5 Å without introducing external force on all water molecules. Interestingly, simulation results indicate that the force on the water molecules inside the channel does not seriously affect the water density distribution and free energy of occupancy fluctuation in the pore (see Figs. 10 and 11). Similar conclusions have also been shown in the paper.[41] From Figs. 10(a) and 11(a), the differences in $\rho(z)$ and $G(N)$ between equilibrium and nonequilibrium are negligible for δ=0. As the nanochannel is deformed, such as δ=2.5 Å, their differences are still small. The water density left to the forced atom increases slightly, while the part right to the forced atom decreases a little.

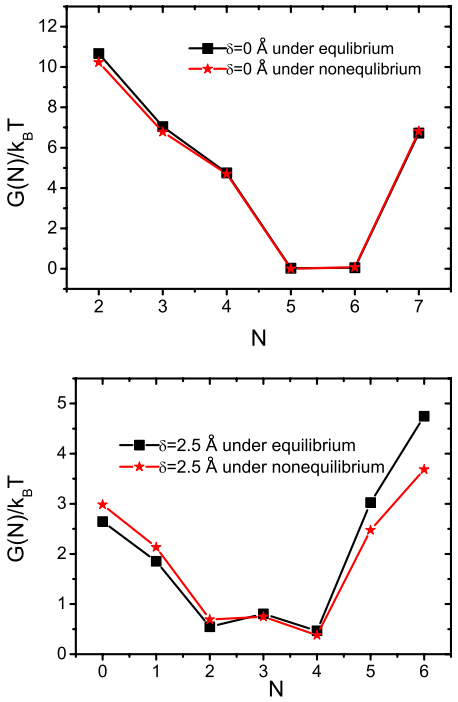

FIG. 11. (Color online) Free energy of occupancy fluctuation $G(N)$ with or without the external artificial osmotic pressure for δ =0 Å and δ=2.5 Å.

IV. THEORETICAL MODEL

Now, we present a theoretical model to understand the wavelike water density distribution observed from molecular dynamics simulation. The model is based on the following three assumptions:

(i) water molecules inside the nanotube form a single-file chain;

(ii) the distance between any two neighboring water molecules inside the nanotube along the z direction is fixed, which is denoted by d;

(iii) the change in free energy of the single-file water inside the nanotube mainly results from the change in water-CNT interaction energy $u(z)$ when the CNT is deformed by the external force.

In this model, the input is the water-CNT interaction energy $u(z)$ (shown in Fig. 8) and the equilibrium distance d between the two neighboring water molecules inside the channel, both of them can be obtained without numerical simulations.

The equilibrium distance between the two water molecules is usually recognized to be about 2.8 Å. However, in this system, considering that the water molecules inside channel usually have a zigzag position distribution along the channel as the typical example (see Fig. 9, top panel), we modify d_{WW} as the distance between the two water molecules along the z direction, which is about 2.6 Å from the simulation. However, this modification does not change the conclusions obtained in this model. Therefore, we choose d=2.6 Å.

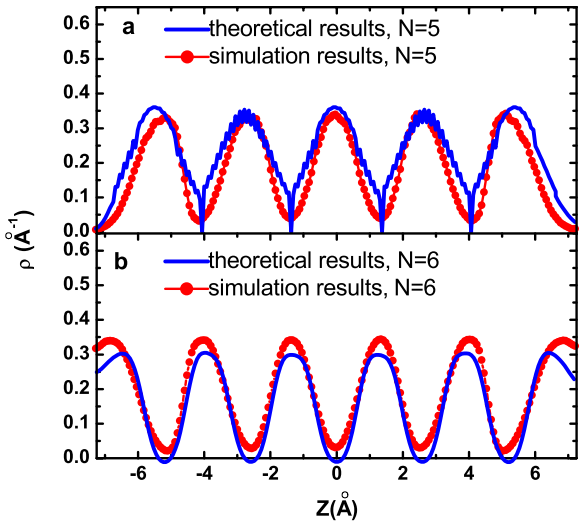

FIG. 12. (Color online) The water probability density distributions along the nanotube axis for (a) $N=5$ and (b) $N=6$ for $\delta=0$.

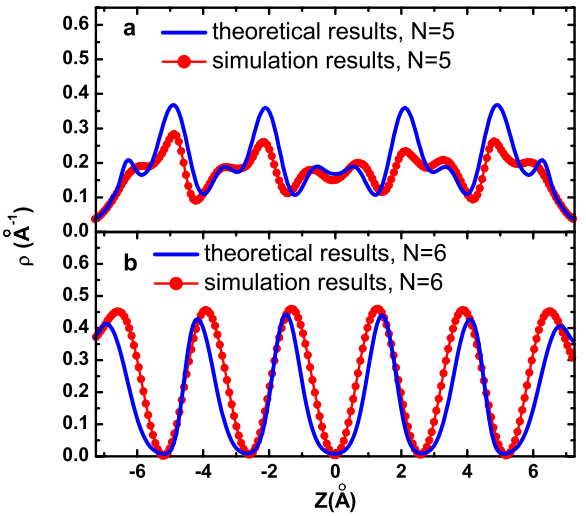

FIG. 13. (Color online) The water probability density distributions along the nanotube axis for (a) $N=5$ and (b) $N=6$ for $\delta=2.1$ Å.

The total potential $U(z)$ of water molecules inside the CNT can be written as a sum over all water molecules,

$$U(z) = \sum_{i=-\infty}^{+\infty} u(z+id) f(z_i), \tag{1}$$

where z is the position of a water molecule (denoted by P_0). $i>0$ indicates that the water molecule locates in the right side of the P_0 and vice versa. $f(z_i)$ is a truncation function which is given by

$$f(z_i) = \begin{cases} 1 & \text{if } z_{\min} \le z_i \le z_{\max}, \\ 0 & \text{if } z_i < z_{\min}, z_i > z_{\max}, \end{cases}$$

where $z_{\min}$ and $z_{\max}$ are the z positions of the left and right ends of the CNT, respectively.

The probability density of water molecules appearing at position z can be assumed as

$$\rho(z) = A \exp[-U(z)/k_B T], \tag{2}$$

where k_B is the Boltzmann constant, T is the temperature of the system, and A can be determined by the average number of water molecules in the CNT,

$$\langle N \rangle = \int_{z_{\min}}^{z_{\max}} \rho(z) dz.$$

We can now calculate the probability density of the representative systems.

Figure 12 shows the comparison between the theoretical results and the simulation results of the water probability density distribution for the unperturbed channel. The curves of the theoretical results in the cases of $N=5,6$ have five and six troughs, respectively, consisting with the simulation results very well. The peaks of the curves of the theoretical results are a little sharper than that of the simulation results. The main reason for this is that d in the model is assumed to be a constant (hard-sphere assumption), while in simulations, the distance between a pair of neighboring water molecules can change according to the interaction potential between those two neighboring water molecules.

We also show the theoretical predictions together with the numerical simulation results in Fig. 13 for $\delta=2.1$ Å. It is clear that the deformation greatly changes the water distribution inside the channel for $N=5$, while slightly for $N=6$. Moreover, the peaks from the theoretical prediction are much higher than the numerical simulations for $N=5$, which shows that there are relatively large errors in the theoretical predictions.

We note that in our model, d is assumed to be fixed as 2.6 Å. However, from Fig. 9, it is clear that the distance between the two water molecules just left and right to the forced atom increases very quickly for $\delta > \delta_c$. Consequently, as δ further increases from δ_c, the error of the theoretical prediction increases very quickly. The theoretical model cannot reflect the key points of the system for a larger deformation parameter δ.

V. CONCLUSIONS

We have studied the gating of water permeation across and the patterns of the density distribution of water inside the nanochannels with appropriate radii under continuous deformations by molecular dynamics simulations, where the water molecules form single files inside the nanochannels. When the number of water molecules inside the channel N is close to 5.5, which is in contrast to the previous result of $N=5$, there is no clearly wavelike pattern for the water density distribution near the center of the channel. However, we find that the water density distribution still exhibits clear wavelike pattern if we collect the data only for the case that the number of water molecules inside the nanochannel is fixed to a value of 5 or 6. Only when the water density distribution of the wavelike pattern of either state of N to be 5 or 6 is

considerably deformed, the net flux across the channel shows clear and sharp decrease. This indicates that the change in the water permeation across the channel, which shows gating effect, is consistent with the behavior of the changes in those wavelike water patterns of particular value of N as the deformation increases. The finding indicates that both the gating and wavelike pattern are independent of the lengths of the nanochannels.

A simple theoretic model is proposed to explore the physics behind the wavelike structure of water density distributions along the channel. We find that the potential barriers at both ends together with the tight hydrogen-bonding network inside the tube and the nanoscale confinement are the main responsibility.

ACKNOWLEDGMENTS

We thank Chunlei Wang, Songyan Li, and Zhaoxia Li for helpful discussions. This work was supported by grants from the Chinese Academy of Sciences, the National Science Foundation of China under Grant No. 10674146, the National Basic Research Program of China under Grants No. 2006CB933000 and No. 2006CB708612, and the Shanghai Supercomputer Center of China.

*Corresponding author; fanghaiping@sinap.ac.cn

[1] S. Iijima, Nature (London) **354**, 56 (1991).
[2] K. B. Jirage, J. C. Hulteen, and C. R. Martin, Science **278**, 655 (1997).
[3] A. Srivastava, O. N. Srivastava, S. Talapatra, R. Vajtai, and P. M. Ajayan, Nat. Mater. **3**, 610 (2004).
[4] D. S. Sholl and J. K. Johnson, Science **312**, 1003 (2006).
[5] S. Ghosh, A. K. Sood, and N. Kumar, Science **3**, 610 (2006).
[6] Y. Liu and Q. Wang, Phys. Rev. B **72**, 085420 (2005).
[7] B. C. Regan, S. Aloni, R. O. Ritchie, U. Dahmen, and A. Zettl, Nature (London) **428**, 924 (2004).
[8] K. Besteman, J.-O. Lee, F. G. M. Wiertz, H. A. Heering, and C. Dekker, Nano Lett. **3**, 727 (2003).
[9] A. Striolo, Nano Lett. **6**, 633 (2006).
[10] H. Gao, Y. Kong, and D. Cui, Nano Lett. **3**, 471 (2003).
[11] J. K. Holt, H. G. Park, Y. Wang, M. Stadermann, A. B. Artyukhin, C. P. Grigoropoulos, A. Noy, and O. Bakajin, Science **312**, 1034 (2006).
[12] T. D. Yuzvinsky, W. Mickelson, S. Aloni, S. L. Konsek, A. M. Fennimore, G. E. Begtrup, A. Kis, B. C. Regan, and A. Zettl, Nano Lett. **6**, 2718 (2006).
[13] D. J. Mann and M. D. Halls, Phys. Rev. Lett. **90**, 195503 (2003).
[14] K. Koga, G. T. Gao, H. Tanaka, and X. C. Zeng, Nature (London) **412**, 802 (2001).
[15] K. Koga, R. D. Parra, H. Tanaka, and X. C. Zeng, J. Chem. Phys. **113**, 5037 (2000).
[16] S. M. Saparov, J. R. Pfeifer, L. Al-Momani, G. Portella, B. L. de Groot, U. Koert, and P. Pohl, Phys. Rev. Lett. **96**, 148101 (2006).
[17] R. Allen, S. Melchionna, and J.-P. Hansen, Phys. Rev. Lett. **89**, 175502 (2002).
[18] S. Andreev, D. Reichman, and G. Hummer, J. Chem. Phys. **123**, 194502 (2005).
[19] F. Zhu and K. Schulten, Biophys. J. **85**, 236 (2003).
[20] R. Z. Wan, J. Y. Li, H. J. Lu, and H. P. Fang, J. Am. Chem. Soc. **127**, 7166 (2005).
[21] J. Y. Li, X. J. Gong, H. J. Lu, H. P. Fang, and R. Zhou, Proc. Natl. Acad. Sci. U.S.A. **104**, 3687 (2007).
[22] K. Murata, K. Mitsuoka, T. Hirai, T. Walz, P. Agre, J. B. Heymann, A. Engel, and Y. Fujiyoshi, Nature (London) **407**, 599 (2000).
[23] B. L. de Groot and H. Grubmüller, Science **294**, 2353 (2001).
[24] G. M. Preston and P. Agre, Proc. Natl. Acad. Sci. U.S.A. **88**, 11110 (1991).
[25] O. Beckstein, P. C. Biggin, and M. S. P. Sansom, J. Phys. Chem. B **105**, 12902 (2001).
[26] P. Gallo, M. Rovere, and E. Spohr, J. Chem. Phys. **113**, 11324 (2000).
[27] L. Kullman, M. Winterhalter, and S. M. Bezrukov, Biophys. J. **82**, 803 (2002).
[28] M. Jensen, S. Park, E. Tajkhorshid, and K. Schulten, Proc. Natl. Acad. Sci. U.S.A. **99**, 6731 (2002).
[29] G. Hummer, J. C. Rasaiah, and J. P. Noworyta, Nature (London) **414**, 188 (2001).
[30] J. Liu *et al.*, Science **280**, 1253 (1998).
[31] D. W. Brenner, Phys. Rev. B **42**, 9458 (1990).
[32] J. Tersoff, Phys. Rev. Lett. **61**, 2879 (1988).
[33] F. Zhu, E. Tajkhorshid, and K. Schulten, Biophys. J. **83**, 154 (2002).
[34] S. Joseph and N. R. Aluru, Nano Lett. **8**, 452 (2008).
[35] www.gromacs.org
[36] H. J. C. Berendsen, J. P. M. Postma, W. F. van Gunsteren, A. D. Nola, and J. R. Haak, J. Chem. Phys. **81**, 3684 (1984).
[37] W. L. Jorgensen, J. Chandrasekhar, J. D. Madura, R. W. Impey, and M. L. Klein, J. Chem. Phys. **79**, 926 (1983).
[38] M. L. Zeidel, S. V. Ambudkar, B. L. Smith, and P. Agre, Biochemistry **31**, 7436 (1992).
[39] P. H. Nelson, J. Chem. Phys. **119**, 6981 (2003).
[40] D. Frenkel and B. Smit, *Molecular Simulation: From Algorithms to Applications* (Harcourt, San Diego, 1996).
[41] F. Zhu, E. Tajkhorshid, and K. Schulten, Phys. Rev. Lett. **93**, 224501 (2004).